

RESEARCH ARTICLE

A Tunable Open Planar Acoustic Notch Filter Utilizing a Pneumatically Modulated Helmholtz Resonator Array

FUMIYA MIZUKOSHI AND HIDETOSHI TAKAHASHI , (Member, IEEE)

Department of Mechanical Engineering, Faculty of Science and Technology, Keio University, Yokohama, Kanagawa 223-8522, Japan

Corresponding author: Hidetoshi Takahashi (htakahashi@mech.keio.ac.jp)

This work was supported by the Keio University Global Research Institute (KGRI)/IoT Healthcare Research Consortium.

ABSTRACT Acoustic filters provide sound insulation unpleasant noises at a specific frequency only. Ordinary passive acoustic filters made up of acoustic metamaterial structures can work without a power supply. However, their working frequency is not adjustable. This study reports a tunable open planar acoustic notch filter that incorporates a pneumatically controlled Helmholtz resonator (HR) array. The HR array consisted of three layers: cavities, a membrane, and microchannels. The cavities function as the HR chambers, whose volume determines the resonant frequency. The acoustic wave is effectively attenuated at this frequency owing to the HR effect. The HR chamber volume can be varied by displacing the stretchable membrane with air pressure through the microchannels. This helps in adjusting the resonant frequency, thereby realizing a tunable acoustic notch filter. We conducted theoretical, and experimental examinations along with simulations of the frequency response for an HR array with three different cavity thicknesses. The prototype device realized a frequency tuning of approximately 4.1–4.9 kHz with 10 dB filtering. Furthermore, an improved notch frequency tunability was observed for the thinner cavities, along with a decrease in the notch performance. Thus, the proposed HR array filter can be useful for high-frequency noise that is generally uncomfortable for humans.


INDEX TERMS Acoustic filter, Helmholtz resonator, passive noise control, pneumatic actuator, soundproof.

I. INTRODUCTION

Acoustic filters are expected to block noise at a specific frequency in residential areas and worksites (Figure 1(a)). Among them, acoustic notch filters can insulate only the unpleasant noise with sharp peaks at specific frequencies, such as those from rotating motors, periodic magnetic fields, or natural vibrations of structures, without disturbing important sounds such as speech and alerts.

Various sound insulation technologies such as passive noise control (PNC) and active noise control (ANC) have been developed. PNC is based on physical sound insulation with sound insulating materials without a power supply. On the other hand, ANC attenuates acoustic noise by

generating canceling waves from a loudspeaker. Electronically controlled ANC allows for complex functions, such as transmitting only voices. Furthermore, recent studies have shown that the improved algorithms have increased the processing speed, enabling their applications to the higher frequencies and the larger spaces [1], [2], [3], [4], [5]. In addition to this, ANC has been employed for open windows, allowing air flows with an array of speakers and microphones [6], [7], [8]. However, in principle, ANC's performance is poor for high-frequency noise owing to the limitations in processing speed. Meanwhile, conventional PNC can provide sound insulation over a wide frequency range without a power supply. However, it is impossible to adjust the filtering frequency and PNC must be sealed to stop the air flow. Therefore, a tunable open passive acoustic filter is necessary.

The associate editor coordinating the review of this manuscript and approving it for publication was Cheng Chin .

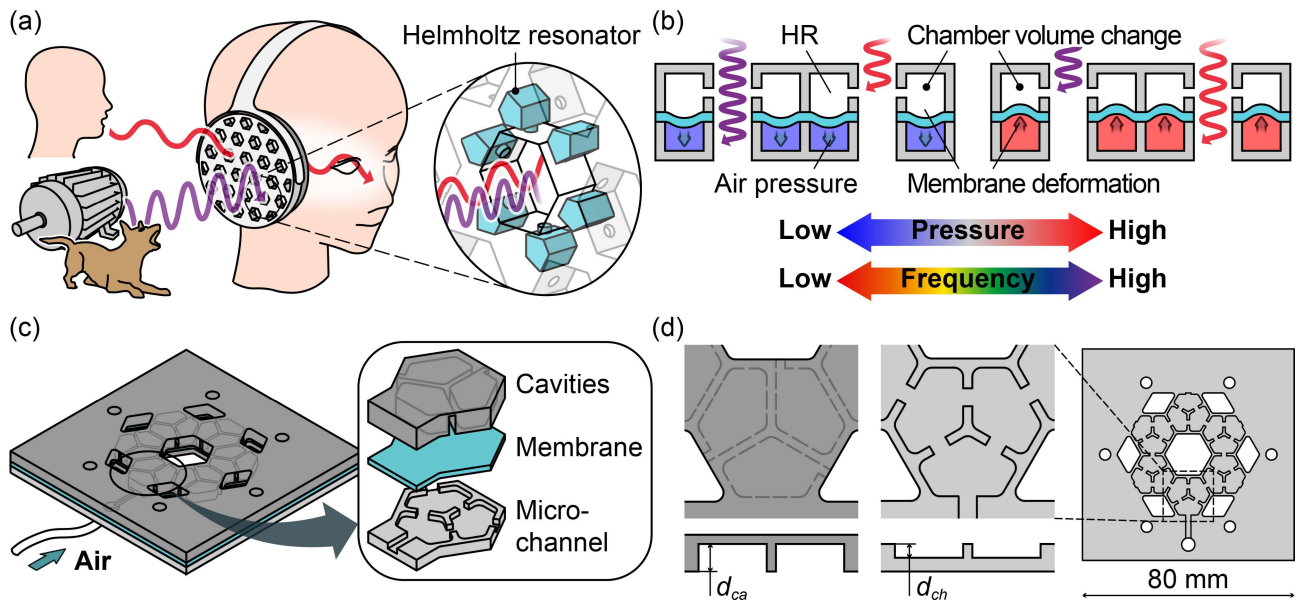


FIGURE 1. (a) Concept sketch of a tunable acoustic notch filter utilizing the HR array. (b) The HR chamber size variations attained by membranes deforming because of pressurized air. The resonant frequency of the HR shifts up and down when positive and negative pressures are applied, respectively. (c) A schematic image of the proposed device wherein the air pressure is applied through a tube to the microchannel. (d) An expanded view of the cavity and microchannel layers. (e) The overall view of the microchannel layer.

In contrast, materials with the designed microscale structures provide superior acoustic properties and have recently gained attention as acoustic metamaterials [9], [10], [11], [12], [13]. Compared to ANC, such metamaterials exhibit special acoustic characteristics without a power supply and do not require a complex system. In particular, some proposed open acoustic metamaterials provide both sound insulation and air ventilation [14], [15], [16], [17], [18]. Furthermore, a recent study has shown that acoustic metamaterials with adjustable structures or membrane tension enable the tuning of working frequency [19], [20], [21], [22], [23], [24], [25]. However, a large structure is needed for a high tunability. Further, it is difficult to implement it in a planar acoustic filter. In contrast, the MEMS pneumatic actuators, which achieve high power and force densities at the microscale level, have been applied in various fields, including the biomedical field [26], [27], [28]. The pneumatic actuators can store energy as pressure, that can be used for tuning. In addition to this, they work on a simple actuation principle. They can be easily integrated into fine and complex structures. Some previous works can be found which presented such concepts and results of closed-acoustic absorbers or insulators using such MEMS technology [29], [30]. Therefore, we applied this MEMS pneumatic technology to actuate the microscale acoustic metamaterials to tune the working frequency of open acoustic filters.

In this study, we propose a tunable acoustic notch filter for uncomfortable sound using a Helmholtz resonator (HR) array. The proposed structure has a high aperture ratio. It offers a permeability of non-target sounds and air ventilation. Moreover, the pneumatically actuated deforming membrane is used for tuning its notch frequency

(Figure 1(b)). The HR, consisting of a chamber with a neck-shaped orifice (neck), has a muffling effect around the resonant frequency. They have been utilized in the acoustic filters and absorbers in the previous studies [31], [32], [33], [34]. The resonant frequency can be selected by changing the HR dimensions. Thus, we can design the appropriate acoustic filter to achieve the desired sound insulation effect. Previously, our team proposed a tunable acoustic notch filter utilizing a pneumatic actuator [35]. This tuning technology has expanded the possible applications of open acoustic filters. In this study, we theoretically analyzed the transmission of the HR array filter using the transfer-matrix method. Furthermore, we examined the HR array with thin cavities to improve the tunability of the filter. The HR array with three different cavity thicknesses was investigated.

II. DESIGN AND THEORETICAL STUDY

The proposed HR array consisted of three layers: the cavities, membranes, and microchannels. The cavities and microchannels sandwich the stretchable membrane, as shown in the Figure 1(c). A slit hole was formed on the side of each cavity as in the HR neck. A significant notch filter was achieved by arranging the six HR arrays in parallel on the side of one acoustic path hole. All the microchannels were connected, and the air pressure was applied uniformly to each membrane. Applying air pressure to the microchannels deforms the membrane and changes the chamber volume. This helps in adjusting the resonant frequency.

Figure 1(d) shows the design of the cavity and channel layers. The cavity and channel was fabricated using 4 mm and 3 mm thick stainless-steel sheets, respectively. The HRs are designed to have a resonant frequency of

approximately 5 kHz when no pressure is applied. A frequency of 5 kHz is uncomfortable for the humans. We determined the dimensions of the HR array to have an aperture ratio of approximately 0.3 for other sound permeability and air ventilation. We designed three cavities with depths of 1 mm, 2 mm, and 3 mm. Each cavity volume was $V_{ca} = 50 \text{ mm}^3$, 100 mm^3 , and 150 mm^3 . Each neck aperture area was $A_h = 1 \text{ mm}^2$, 2 mm^2 , and 3 mm^2 . All the cavities were having a same neck length l_0 of 1 mm. The thinner the cavity, the greater the volume change rate owing to membrane deformation. This increases the tunable range of the resonant frequency. The membrane seals each cavity to form an HR chamber. A 1 mm thick silicone rubber sheet was used as the membrane. The membrane displaces by approximately $\pm 1.5 \text{ mm}$ with $\pm 100 \text{ kPa}$ air pressure. Further, the HR chamber volume changes by approximately $\pm 40 \text{ mm}^3$. When no pressure is applied, the resonant frequency of the HR array with a 3 mm thick cavity is calculated as $f_0 = 4.74 \text{ kHz}$ using the following equation:

$$f_0 = \frac{c}{2\pi} \sqrt{\frac{A_h}{l_h V_{ca}}} \quad (1)$$

where the speed of sound in air is $c = 343 \text{ m/s}$, and l_h is the actual HR neck length corrected as $l_h = l_0 + l_e$, considering the end correction. l_e is calculated as $l_e = 2l_{ee}$, where l_{ee} is the end correction for one side of the neck. In this case, the neck aperture is rectangular. However, the end correction of the HR is calculated for the circular neck aperture [36]. Thus, assuming the neck aperture to be a circle of the same area, the neck radius $r_h = \sqrt{A_h/\pi}$ is converted and then substituted into the correction equation as follows:

$$l_{ee} = \frac{8r_h}{3\pi} \quad (2)$$

In addition to this, the change in the chamber volume because of the membrane deformation shifts the resonant frequency to approximately 4–5 kHz. The overall design of the microchannel is shown in the Figure 1(d) (right). Eighteen HRs were placed in the center of a 80 mm square plate. The hexagonal holes and HRs were arranged in a honeycomb structure with an aperture area ratio of 1:2. All the microchannels were connected to an outer conduit, and the air pressure was applied through a silicon tube.

We theoretically analyzed the transmission loss of the HR array filter using the transfer-matrix method. When the HRs were mounted on a penetration hole, the incident acoustic wave was drastically reduced at the resonant frequency. Figure 2(a) represents a theoretical model with parameters: the penetration hole's first half-length l_{f1} , second half-length l_{f2} , cross-sectional area A_1 , HR chamber volume V_h , HR neck length l_h , and cross-sectional area A_h . The acoustic pressure p and the volumetric flow rate Q at five points, the inlet and outlet of the first and second half hole and at the HR neck, are marked with subscripts 1, 2, 3, 4, and h , respectively, in the figure.

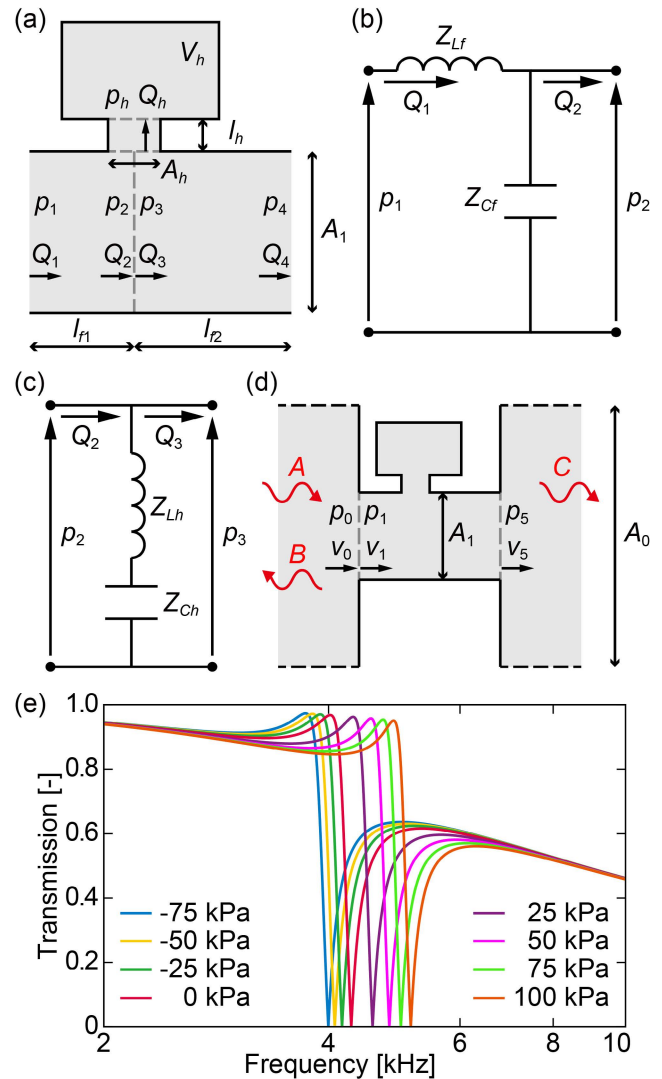


FIGURE 2. (a) Theoretical model of the HR mounted on the penetration hole. Electrical circuit analogous to (b) a half penetration hole and (c) a HR. (d) A unit of the HR array filter against the vertically incident acoustic wave. (e) Acoustic transmission of the HR array filter calculated with the transfer matrix method. For each pressure, the experimentally measured chamber volumes were substituted for the calculations; 172 mm^3 for -75 kPa , 166 mm^3 for -50 kPa , 159 mm^3 for -25 kPa , 150 mm^3 for 0 kPa , 131 mm^3 for 25 kPa , 118 mm^3 for 50 kPa , 110 mm^3 for 75 kPa , and 104 mm^3 for 100 kPa .

The effect of the viscous loss should be considered when the acoustic filter has a microscale structure. Viscous losses were the most pronounced in the HR neck at the resonant frequency. The boundary layer thickness d_v is expressed as follows:

$$d = \sqrt{2\eta/\rho_f \omega} \quad (3)$$

where η is the dynamic viscosity, ρ_0 is the equilibrium medium density, and ω is the angular frequency. When the dynamic viscosity and density of air were $\eta = 18.13 \times 10^{-6} \text{ Pa}\cdot\text{s}$ and $\rho_f = 1.166 \text{ kg/m}^3$, respectively, $d = 0.0457 \text{ mm}$ was calculated at the resonance frequency $f_0 = 4.74 \text{ kHz}$. This diameter was sufficiently smaller than the

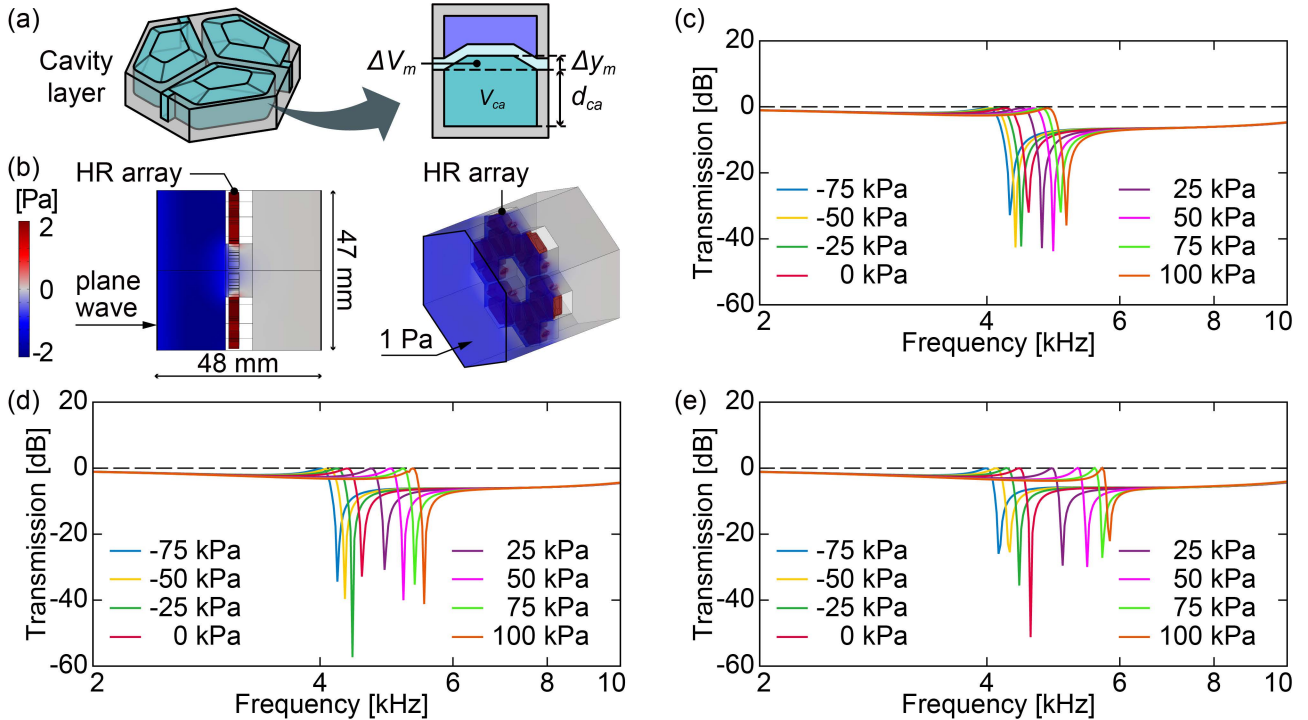


FIGURE 3. (a) Simulation model of HR array unit. Here, the light blue area functions as HR, and the chamber volume change because of membrane deformation is approximated by a pentagonal frustum. (b) Cross-sectional and perspective views of the simulation model. The Pressure distribution at the notch frequency (4.54 kHz) is shown. Simulated frequency response of the HR array with cavities of (c) 3 mm, (d) 2 mm, and (e) 1.5 mm thickness.

diameter of the pipe at the neck, indicating that the effect of viscous loss was negligible.

This acoustic system can be represented as an analogous electrical circuit model by assuming that the overall dimensions of the structure are significantly smaller than the wavelength. The first half-penetration hole is represented in Figure 2(b) as an electrical circuit. The acoustic mass and stiffness in this system are represented as $L_{f1} = \rho_f l_{f1} / A_1$ and $C_{f1} = A_1 l_{f1} / B_f$, respectively, where B_f is the bulk modulus of air. The acoustic impedances of the inductance and capacitance in the equivalent electrical circuit in Figure 2(b) are given as $Z_{L_{f1}} = j\omega L_{f1}$ and $Z_{C_{f1}} = 1 / j\omega C_{f1}$, respectively. Here, we introduce the state vector $\mathbf{W}_n = (p_n \ Q_n)^T$ with any subscript n, and the transfer matrix relation between two points as $\mathbf{W}_m = T \ \mathbf{W}_n$. The transfer matrix between the inlet and outlet of the first-half penetration hole can be obtained as

$$T_{f1} = \begin{bmatrix} 1 + Z_{L_{f1}}/Z_{C_{f1}} & Z_{L_{f1}} \\ 1/Z_{C_{f1}} & 1 \end{bmatrix}, \quad (4)$$

where $\mathbf{W}_1 = T_{f1} \ \mathbf{W}_2$. Similarly, the transfer matrix relation, $\mathbf{W}_3 = T_{f2} \ \mathbf{W}_4$, is obtained for the second-half penetration hole. Then, in the HR, the neck and chamber function as the mass and spring, neglecting the viscous loss from the above discussion. $M_h = \rho_f l_h A_h$ and $K_h = B_f A_h^2 / V_h$ are the mass and stiffness of the HR, respectively. The acoustic impedance of the HR can be given as $Z_h = Z_{lh} + Z_{ch}$, where $Z_{lh} = K_h / j\omega A_h^2$ and $Z_{ch} = j\omega M_h / A_h^2$ are the impedances

of the inductance and capacitance in the equivalent electrical circuit shown in Figure 2(c), respectively. Here, six HRs are attached in parallel on the sides of the penetration hole; hence, the overall acoustic impedance of the six HRs is calculated as $Z_{h6} = Z_h / 6$. From these equations, the transfer matrix relation $\mathbf{W}_2 = T_{h6} \ \mathbf{W}_3$ can be obtained, where T_{h6} is represented as:

$$T_{h6} = \begin{bmatrix} 1 & 0 \\ 1/Z_{h6} & 1 \end{bmatrix}. \quad (5)$$

From Eqs. (4) and (5), the overall transfer matrix of the HR array unit can be expressed as:

$$T = T_{f1} T_{h6} T_{f2}. \quad (6)$$

Subsequently, the transmittance of the HR array filter for a vertically incident wave was calculated. In Figure 2(c), A_0 is the occupancy area of one unit, and the aperture ratio $r = A_1 / A_0$ needs to be calculated. We set the complex amplitudes of the incident, reflected, and transmitted waves as A , B , and C , respectively. The acoustic pressure and particle velocity at the front and back of the HR array filter are represented as

$$\begin{pmatrix} p_0 \\ v_0 \end{pmatrix} = \begin{pmatrix} j\omega\rho \{Ae^{j\omega t} + Be^{j\omega t}\} \\ jk \{Ae^{j\omega t} - Be^{j\omega t}\} \end{pmatrix}, \quad (7)$$

$$\begin{pmatrix} p_5 \\ v_5 \end{pmatrix} = \begin{pmatrix} j\omega\rho Ce^{j\omega t} \\ jkCe^{j\omega t} \end{pmatrix}, \quad (8)$$

where k is the wavenumber. Considering the boundary condition and constant volumetric flow rate, the following

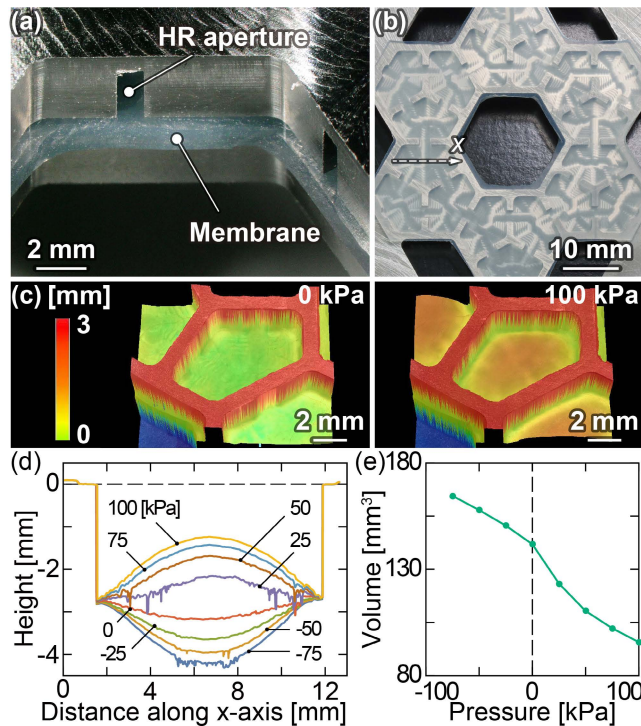


FIGURE 4. Photographs of (a) the aperture in the fabricated HR array and (b) the assembled membrane and microchannel layers. (c) Measurement results; (d) profiles; and (e) variation in HR chamber volume change resulting from membrane deformation with air pressure.

equations can be obtained using the aperture ratio: $(p_0 v_0)^T = (p_1 r v_1)^T$ and $(p_5 v_5)^T = (p_4 r v_4)^T$. Substituting Eqs. (6), (7), and (8) into the above, we can obtain the acoustic transmission of the HR array filter, $|C/A|$.

We calculated the transmission of the HR array filter with a 3 mm thick cavity at 2–10 kHz (Figure 2(e)). The following values of the parameters were used: $A_0 = 210 \text{ mm}^2$, $A_1 = 631 \text{ mm}^2$, $l_{f1} = 2.5 \text{ mm}$, $l_{f2} = 5.5 \text{ mm}$, $A_h = 3 \text{ mm}^2$, and $l_h = 3.26 \text{ mm}$. The chamber volume V_h was varied from 150 mm^3 at no pressure from -46 – 22 mm^3 , which was obtained in the experiment with air pressure in the range of -75 – 100 kPa (see below in the later chapter). The transmission decreased rapidly at the resonant frequency, and shifted by 4.00 – 5.16 kHz when the chamber volume changed. The notch filtering effect of the HR array was theoretically confirmed. However, when the cavity is thinner, the chamber shape deviates from the ideal shape, and the calculated values are far from the experimental values (mentioned in APPENDIX and Figure 6). Hence, the finite-element method (FEM) was used to analyze the filtering effect of the HR array more accurately.

III. ACOUSTIC SIMULATIONS

We calculated the acoustic characteristics of the proposed structure using a simulation software (COMSOL Multiphysics 6.0, COMSOL, USA). The simulations were performed using HR array models with 3, 2, and 1.5 mm thick cavities. A pentagonal frustum model was used to

approximate the change in the chamber volume ΔV_m because of membrane deformation (Figure 3(a)), which varied in the range of -46 – 22 mm^3 . The total chamber volume, $V_h = V_{ca} + \Delta V_m$, was varied according to ΔV_m and the cavity volume V_{ca} , which was set to 150, 100, and 75 mm^3 for each of the thick cavities. Figure 3(b) depicts the simulation model. The hexagonal prismatic region was used as the computational region, and periodic boundary conditions were set on the six side surfaces. The incident and radiation plane-wave conditions were set at the front and back surfaces of the region.

The simulated frequency response in the range of 2–10 kHz is shown in Figure 3(c–e). The acoustic transmission was calculated using the acoustic pressure and particle velocity at the center point of the front and back surfaces. A sharp decrease at the resonant frequency due to the HR effect was evident in the spectra. Moreover, the resonant frequency shifted as the volume of the HR chamber changed. The simulation results indicated that the notch frequency of the HR array filter with a 3 mm thick cavity varied in the range of 4.29–5.10 kHz for an air pressure of -75 – 100 kPa (Figure 3(c)). Furthermore, the notch in the graph was smaller when the chamber volume was smaller, because the extremely thin geometry of the HR chamber prevented the resonant effect. This phenomenon was more apparent when a higher pressure was applied to the HR array filter with a 1.5 mm thick cavity.

IV. MEMBRANE DEFORMATION

The fabricated HR array filter is shown in Figure 4(a). A 1 mm thick flat silicone membrane was placed between the stainless-steel cavities and the microchannel housings. Figure 4(b) shows a photographic image of the entire membrane and microchannel layers. The microchannel was connected to a pressure calibrator (KAL200, Halstrup-Walcher GmbH) using a silicon tube. An air pressure of -75 – 100 kPa was applied, and the resulting membrane deformation was observed with a microscope (VHX-6000, Keyence). The displacements of the membrane deformation at air pressures of 0 and 100 kPa are shown in Figure 4(c). The membrane was deformed upward by approximately 1.5 mm at an air pressure of 100 kPa. The cross-sectional deformation profiles measured along the centerline of each unit are shown in Figure 4(d). The membrane deformed by $\pm 1.5 \text{ mm}$ in height for air pressures in the range of -75 – 100 kPa . The calculated HR chamber volume shifts are shown in Figure 4(e). The volume was varied from 150 mm^3 to 104 – 172 mm^3 at no pressure.

V. EXPERIMENTAL RESULTS

We experimentally measured the frequency response of the fabricated HR array filter using a speaker (E4000, S'Next Co., Ltd., Japan) and microphone (MI-3170, Ono Sokki Co., Ltd., Japan) (Figure 5(a)). The gains were calculated based on the measurement results corresponding to the model without HRs. The HR array filter with a $d_{ca} = 3 \text{ mm}$ thick cavity had a maximum transmission loss of approximately

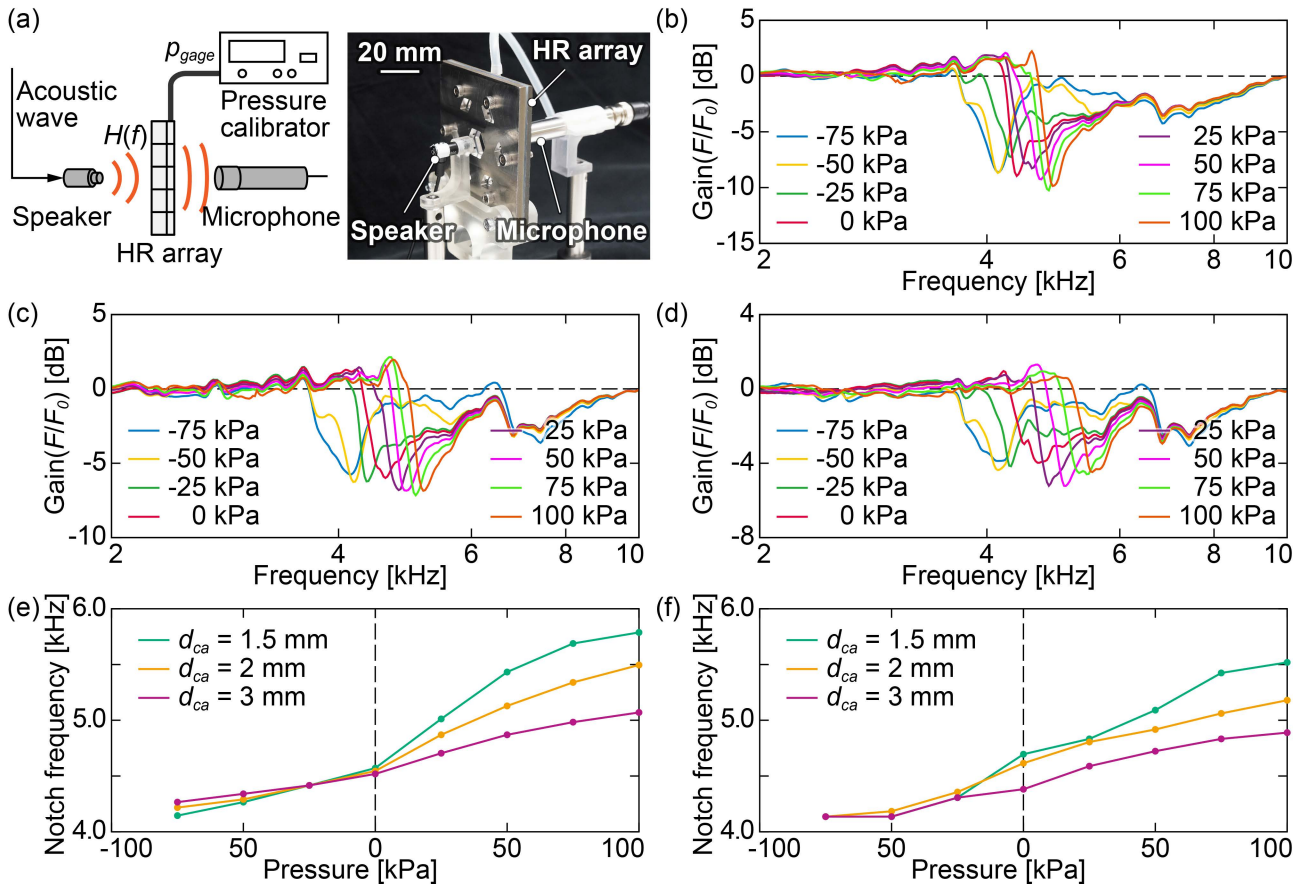


FIGURE 5. (a) Experimental setup. (b) Frequency response of the HR array filter with d_{ca} of (b) 3 mm, (c) 2 mm, and (d) 1.5 mm. Variation of (e) simulated and (f) experimental notch frequency with air pressure. The thinner the d_{ca} , the larger the change in rate of the notch frequency.

10 dB in each case, whereas the notch frequency varied from 4.14 to 4.89 kHz according to air pressure change in the range of -75 – 100 kPa (Figure 5(b)). Furthermore, as the cavity thickness decreased, the notch depth and sharpness decreased and the notch frequency shift range increased. The HR array filter with $d_{ca} = 1.5$ mm had a maximum transmission loss of approximately 4 dB and a notch frequency shift range of 4.14–5.52 kHz. The variation of simulated and experimental notch frequencies with the applied air pressure is shown in Figures 5(e) and (f), respectively. Evidently, the notch frequency shifts more significantly, particularly at the high-pressure side for HR array filters with thinner cavities, where the rate of chamber volume change is large. The notch frequency shifts were most sensitive to pressures of approximately 0–25 kPa. This tendency was consistent between the simulation and experimental results.

VI. DISCUSSION

The proposed notch filter has a frequency tunability of 4.14–5.52 kHz, corresponding to a fractional bandwidth of 28.9%. A similar research had achieved 17% tunability for a pneumatically actuated membrane-type acoustic metamaterial [21]. By contrast, an acoustic metamaterial consisting an array of resonators actuated by dielectric elastomer realized

14% tunability [22]. These acoustic metamaterial membranes can be easily minimized and integrated; however, they exhibit poor tunability compared to metamaterials with adjustable structures [19], [25]. This study proposes an acoustic filter, consisting of a pneumatically actuated HR array with thinner cavities, providing a wide band tunability than the previous study. Furthermore, the proposed structure has a high aperture ratio of 0.3, which offers better ventilation and a sharp notch of transmission.

However, the notch of the fabricated HR array filter was not as sharp as that of the simulated one. The experimental FWHM of the frequency response was approximately 300 Hz compared to the 30 Hz derived in the simulation. This may be due to variations in the dimensions of the fabricated HRs and membrane deformation.

By contrast, the difference in the evaluation method resulted in a discrepancy between the simulated and experimental spectra. The acoustic transmission was calculated from the acoustic simulation as described in section III. The simulated spectra were almost consistent with the theoretical ones (presented in APPENDIX). Furthermore, we calculated the gain of the HR array by comparing two measurement results. It slightly deviated from the ideal transmission due to reflection and the fact that the acoustic source is not a

perfect plane-wave source unlike assumed in the simulation. In addition, simulations were performed (APPENDIX) under conditions for a point acoustic source similar to the experimental one. These results confirmed that the experimental spectrum exhibited a blend of simulated spectra under two different conditions. This suggests that the acoustic source used in the experiment has a form between a point and a plane. Nevertheless, the experimental and the simulated notch spectrum of the HR array were similar.

The notch frequencies obtained via theory, simulation, and experiment differed slightly. This may be because of dimensional errors introduced during the fabrication and inaccuracy in the aperture correction of the HR. Notably, the aperture correction (equation 2) assumed circular neck apertures [36]. Moreover, the notch frequency for the HR with a thin cavity could not be calculated accurately from the theoretical model (described in APPENDIX). In cases where the HR chamber and neck have a complicated geometry, complex theoretical models are required to determine the end correction [37], [38], [39]. In future studies, these considerations will be required to develop an optimal design for HR arrays.

In this study, we examined the performance of an HR array against vertically incident waves. Analyses of obliquely incident waves have already been performed for acoustic metamaterials [14], [15]. Although the effectiveness and tunability of the HR array filter were confirmed, further studies should be conducted to gain deeper insights.

In addition, when the unit number and area of the HR array filter are increased, the transmission can be influenced by the coincidence effect [40]. In this study, this effect was not observed for the HR array filter on a small scale, but careful consideration is necessary on a large scale.

The advances in fabrication techniques will allow precise and complex structures, which can enable the construction of proposed acoustic filters with a sharper notch at higher frequency, and this may expand the scope of the present study. Meanwhile, such acoustic filter designs may make the effect of viscosity more pronounced. The effects of geometric parameters on viscosity will be analyzed in future studies.

In this study, we developed a tunable acoustic notch filter with an HR array. However, arraying HRs with multiple parameters would extend the insulating frequency bandwidth and could be applied to bandstop filters. In addition, multiple pneumatic actuators would provide tunability of the bandwidth, which could improve the applicability of HR array filters.

VII. CONCLUSION

In this study, a tunable acoustic notch filter that utilizes a pneumatic-deforming HR array was developed. We investigated the frequency response of an HR array with cavities of three different thicknesses using the transfer matrix method, acoustic simulations, and experiments. The notch frequency was tunable in the range of 1 kHz via pneumatic control. Furthermore, thinner cavities improved the tunability of notch frequency while decreasing the notch performance. In the

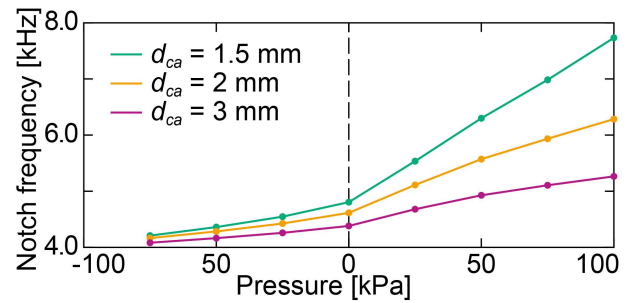


FIGURE 6. Variation in notch frequency with air pressure derived from theoretical study.

experiments, the filtering effect was approximately 10 dB at the notch frequency corresponding to the HR array with the thickest cavity. The proposed acoustic notch filter is effective for noises of a specific frequency in residential spaces and work sites.

APPENDIX

The variation in notch frequencies as a function of the applied air pressure derived from the theoretical study is shown in Figure 6. The notch frequency for the cavity thickness $d_{ca} = 3$ mm shifted from 4.00 to 5.16 kHz as seen from the figure. This is consistent with the simulation and experimental results. However, the notch frequencies for $d_{ca} = 2$ and 1.5 mm, at higher pressure, were far from the simulation and experimental values. This is attributed to the deviation in the HR chamber shape from the ideal sphere due to the thin cavity. Therefore, the Helmholtz resonator formula, equations (1) and (2), cannot be applied. By contrast, acoustic simulations predicted the notch frequency of the HR array for all cavity thicknesses more accurately.

We compared the frequency responses obtained by the acoustic simulations with the transfer matrix method. Figure 7 shows the acoustic transmission obtained from the simulations as described in Section III. It was confirmed that the spectra (Figure 7 (a)) for d_{ca} of 3 mm were similar to that of theoretical ones presented in Figure 2(e); however, increased transmission was obtained for high frequencies from the simulation. This is probably because the simulation did not generate a perfect plane-wave, which is especially true with short wavelengths. In conclusion, these results validated the consistency of the theoretical model and simulations.

In addition, the difference in the simulation and experimental evaluation methods caused the discrepancy in the spectra. We conducted additional simulations under the conditions similar to the experimental setup (section V). The simulation model is shown in Figure 8 (a). A sound point source was positioned at a distance of 5 mm from the center hole of the HR array. The detector was positioned on the opposite side at a distance of 10 mm from the center hole.

The simulated results are shown in Figure 8 (b–d). The gains ($\text{Gain}(H/H_0)$) were calculated based on the simulation results of the model without HRs as in the experiment.

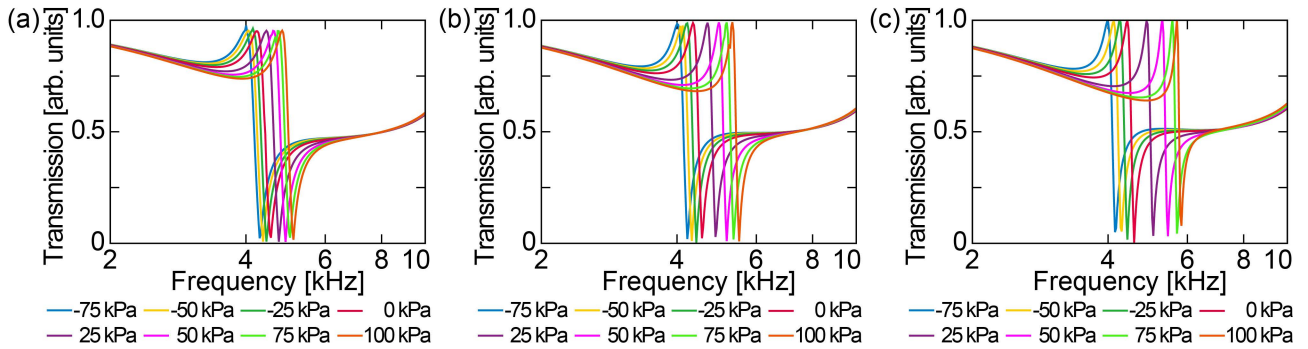


FIGURE 7. Simulated frequency response of the HR array with cavities of (a) 3 mm, (b) 2 mm, and (c) 1.5 mm thickness.

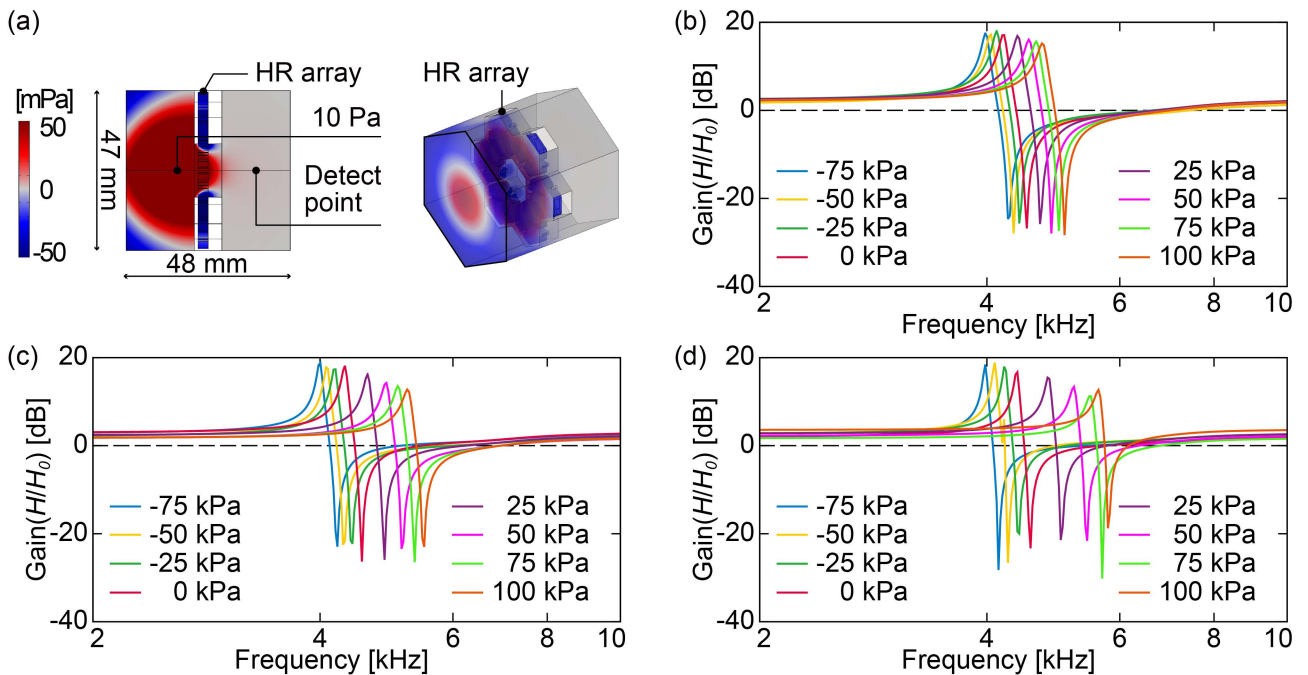


FIGURE 8. (a) A cross-sectional and perspective views of the simulation model similar to the experimental setup. Simulated frequency response of the HR array with cavities of: (b) 3 mm, (c) 2 mm, and (d) 1.5 mm thickness.

A sharp decrease in gains was observed at the resonant frequency of the HR. The peak just before the notch is due to the constructive interference at the HR in the acoustic path. Accordingly, this peak frequency depended on the position of the source and detector. By contrast, in the experiment, the sound from the loudspeaker was expected to be in the form between a point and a plane source. Hence, the experimental frequency response exhibited the blend of spectra depicted in Figures 3 (c-e) and 8 (b-d). Nevertheless, the experimental and simulation notch spectrum of the HR array were similar.

REFERENCES

[1] N. V. George and G. Panda, "A robust filtered-s LMS algorithm for nonlinear active noise control," *Appl. Acoust.*, vol. 73, no. 8, pp. 836–841, 2012, doi: 10.1016/j.apacoust.2012.02.005.
 [2] Z. Qiu, C.-M. Lee, Z. H. Xu, and L. N. Sui, "A multi-resolution filtered-x LMS algorithm based on discrete wavelet transform for active noise control," *Mech. Syst. Signal Process.*, vols. 66–67, pp. 458–469, Jan. 2016, doi: 10.1016/j.ymsp.2015.05.024.

[3] S. Dixit and D. Nagaria, "LMS adaptive filters for noise cancellation: A review," *Int. J. Electr. Comput. Eng.*, vol. 7, no. 5, pp. 2520–2529, Oct. 2017, doi: 10.11591/ijece.v7i5.pp2520-2529.
 [4] H. M. Lee, Z. Wang, K. M. Lim, and H. P. Lee, "A review of active noise control applications on noise barrier in three-dimensional/open space: Myths and challenges," *Fluctuation Noise Lett.*, vol. 18, no. 4, Nov. 2019, Art. no. 1930002, doi: 10.1142/S0219477519300027.
 [5] D. Shi, B. Lam, K. Ooi, X. Shen, and W.-S. Gan, "Selective fixed-filter active noise control based on convolutional neural network," *Signal Process.*, vol. 190, Jan. 2022, Art. no. 108317, doi: 10.1016/j.sigpro.2021.108317.
 [6] T. Murao, C. Shi, W.-S. Gan, and M. Nishimura, "Mixed-error approach for multi-channel active noise control of open Windows," *Appl. Acoust.*, vol. 127, pp. 305–315, Dec. 2017, doi: 10.1016/j.apacoust.2017.06.024.
 [7] B. Lam, D. Shi, W.-S. Gan, S. J. Elliott, and M. Nishimura, "Active control of broadband sound through the open aperture of a full-sized domestic window," *Sci. Rep.*, vol. 10, no. 1, pp. 1–7, Dec. 2020, doi: 10.1038/s41598-020-66563-z.
 [8] H. M. Lee, Y. Hua, Z. Wang, K. M. Lim, and H. P. Lee, "A review of the application of active noise control technologies on Windows: Challenges and limitations," *Appl. Acoust.*, vol. 174, Mar. 2021, Art. no. 107753, doi: 10.1016/j.apacoust.2020.107753.

- [9] N. Fang, D. Xi, J. Xu, M. Ambati, W. Srituravanich, C. Sun, and X. Zhang, "Ultrasonic metamaterials with negative modulus," *Nature Mater.*, vol. 5, no. 6, pp. 452–456, Apr. 2006, doi: [10.1038/nmat1644](https://doi.org/10.1038/nmat1644).
- [10] Z. Liang and J. Li, "Extreme acoustic metamaterial by coiling up space," *Phys. Rev. Lett.*, vol. 108, no. 11, pp. 1–4, Mar. 2012, doi: [10.1103/PhysRevLett.108.114301](https://doi.org/10.1103/PhysRevLett.108.114301).
- [11] L. Zigoneanu, B.-I. Popa, and S. A. Cummer, "Three-dimensional broadband omnidirectional acoustic ground cloak," *Nature Mater.*, vol. 13, no. 4, pp. 352–355, Mar. 2014, doi: [10.1038/nmat3901](https://doi.org/10.1038/nmat3901).
- [12] G. Ma and P. Sheng, "Acoustic metamaterials: From local resonances to broad horizons," *Sci. Adv.*, vol. 2, no. 2, Feb. 2016, Art. no. e1501595, doi: [10.1126/sciadv.1501595](https://doi.org/10.1126/sciadv.1501595).
- [13] N. Jiménez, V. Romero-García, V. Pagneux, and J.-P. Groby, "Rainbow-trapping absorbers: Broadband, perfect and asymmetric sound absorption by subwavelength panels for transmission problems," *Sci. Rep.*, vol. 7, no. 1, pp. 1–12, Oct. 2017, doi: [10.1038/s41598-017-13706-4](https://doi.org/10.1038/s41598-017-13706-4).
- [14] C. Shen, Y. Xie, J. Li, S. A. Cummer, and Y. Jing, "Acoustic metacages for sound shielding with steady air flow," *J. Appl. Phys.*, vol. 123, no. 12, Mar. 2018, Art. no. 124501, doi: [10.1063/1.5009441](https://doi.org/10.1063/1.5009441).
- [15] R. Ghaffarivardavagh, J. Nikolajczyk, S. Anderson, and X. Zhang, "Ultra-open acoustic metamaterial silencer based on fano-like interference," *Phys. Rev. B, Condens. Matter*, vol. 99, no. 2, pp. 1–10, Jan. 2019, doi: [10.1103/PhysRevB.99.024302](https://doi.org/10.1103/PhysRevB.99.024302).
- [16] L. Y. L. Ang, Y. K. Koh, and H. P. Lee, "Plate-type acoustic metamaterials: Evaluation of a large-scale design adopting modularity for customizable acoustical performance," *Appl. Acoust.*, vol. 149, pp. 156–170, Jun. 2019, doi: [10.1016/j.apacoust.2019.01.027](https://doi.org/10.1016/j.apacoust.2019.01.027).
- [17] S. Kumar, T. B. Xiang, and H. P. Lee, "Ventilated acoustic metamaterial window panels for simultaneous noise shielding and air circulation," *Appl. Acoust.*, vol. 159, Feb. 2020, Art. no. 107088, doi: [10.1016/j.apacoust.2019.107088](https://doi.org/10.1016/j.apacoust.2019.107088).
- [18] S. Kumar and H. P. Lee, "Recent advances in acoustic metamaterials for simultaneous sound attenuation and air ventilation performances," *Crystals*, vol. 10, no. 8, pp. 1–22, Aug. 2020, doi: [10.3390/cryst10080686](https://doi.org/10.3390/cryst10080686).
- [19] K. J. B. Lee, M. K. Jung, and S. H. Lee, "Highly tunable acoustic metamaterials based on a resonant tubular array," *Phys. Rev. B, Condens. Matter*, vol. 86, no. 18, Nov. 2012, Art. no. 184302, doi: [10.1103/PhysRevB.86.184302](https://doi.org/10.1103/PhysRevB.86.184302).
- [20] Z. Chen, C. Xue, L. Fan, S.-Y. Zhang, X.-J. Li, H. Zhang, and J. Ding, "A tunable acoustic metamaterial with double-negativity driven by electromagnets," *Sci. Rep.*, vol. 6, no. 1, pp. 1–11, Jul. 2016, doi: [10.1038/srep30254](https://doi.org/10.1038/srep30254).
- [21] F. Langfeldt, J. Riecken, W. Gleine, and O. Von Estorff, "A membrane-type acoustic metamaterial with adjustable acoustic properties," *J. Sound Vib.*, vol. 373, pp. 1–18, Jul. 2016, doi: [10.1016/j.jsv.2016.03.025](https://doi.org/10.1016/j.jsv.2016.03.025).
- [22] X. Yu, Z. Lu, F. Cui, L. Cheng, and Y. Cui, "Tunable acoustic metamaterial with an array of resonators actuated by dielectric elastomer," *Extreme Mech. Lett.*, vol. 12, pp. 37–40, Apr. 2017, doi: [10.1016/j.eml.2016.07.003](https://doi.org/10.1016/j.eml.2016.07.003).
- [23] S. Chen, Y. Fan, Q. Fu, H. Wu, Y. Jin, J. Zheng, and F. Zhang, "A review of tunable acoustic metamaterials," *Appl. Sci.*, vol. 8, no. 9, p. 1480, Aug. 2018, doi: [10.3390/app8091480](https://doi.org/10.3390/app8091480).
- [24] S. Kumar and H. P. Lee, "Recent advances in active acoustic metamaterials," *Int. J. Appl. Mech.*, vol. 11, no. 8, Dec. 2019, Art. no. 1950081, doi: [10.1142/S1758825119500819](https://doi.org/10.1142/S1758825119500819).
- [25] Z.-X. Xu, H.-Y. Meng, A. Chen, J. Yang, B. Liang, and J.-C. Cheng, "Tunable low-frequency and broadband acoustic metamaterial absorber," *J. Appl. Phys.*, vol. 129, no. 9, Mar. 2021, Art. no. 094502, doi: [10.1063/5.0038940](https://doi.org/10.1063/5.0038940).
- [26] F. A. M. Ghazali, M. N. Hasan, T. Rehman, M. Nafea, M. S. M. Ali, and K. Takahata, "MEMS actuators for biomedical applications: A review," *J. Micromech. Microeng.*, vol. 30, no. 7, Jul. 2020, Art. no. 073001, doi: [10.1088/1361-6439/ab8832](https://doi.org/10.1088/1361-6439/ab8832).
- [27] M. De Volder and D. Reynaerts, "Pneumatic and hydraulic microactuators: A review," *J. Micromech. Microeng.*, vol. 20, no. 4, Mar. 2010, Art. no. 043001, doi: [10.1088/0960-1317/20/4/043001](https://doi.org/10.1088/0960-1317/20/4/043001).
- [28] S. Nishita and H. Onoe, "Liquid-filled flexible micro suction-controller array for enhanced robotic object manipulation," *J. Microelectromech. Syst.*, vol. 26, no. 2, pp. 366–375, Apr. 2017, doi: [10.1109/JMEMS.2017.2651882](https://doi.org/10.1109/JMEMS.2017.2651882).
- [29] T. Bravo, C. Maury, and C. Pinhède, "Enhancing sound absorption and transmission through flexible multi-layer micro-perforated structures," *J. Acoust. Soc. Amer.*, vol. 134, no. 5, pp. 3663–3673, Dec. 2013, doi: [10.1121/1.4821215](https://doi.org/10.1121/1.4821215).
- [30] M. Yoda and S. Konishi, "Acoustic impedance control through structural tuning by pneumatic balloon actuators," *Sens. Actuators A, Phys.*, vol. 95, nos. 2–3, pp. 222–226, Jan. 2002, doi: [10.1016/S0924-4247\(01\)00729-4](https://doi.org/10.1016/S0924-4247(01)00729-4).
- [31] A. Isozaki, H. Takahashi, H. Tamura, T. Takahata, K. Matsumoto, and I. Shimoyama, "Parallel Helmholtz resonators for a planar acoustic notch filter," *Appl. Phys. Lett.*, vol. 105, no. 24, pp. 2–6, 2014, doi: [10.1063/1.4904509](https://doi.org/10.1063/1.4904509).
- [32] S. H. Lee, B. S. Kang, G. M. Kim, Y. R. Roh, and M. K. Kwak, "Fabrication and performance evaluation of the Helmholtz resonator inspired acoustic absorber using various materials," *Micromachines*, vol. 11, no. 11, p. 983, Oct. 2020, doi: [10.3390/mi11110983](https://doi.org/10.3390/mi11110983).
- [33] F. Mizukoshi and H. Takahashi, "Acoustic notch filtering earmuff utilizing Helmholtz resonator arrays," *PLoS ONE*, vol. 16, no. 10, Oct. 2021, Art. no. e0258842, doi: [10.1371/journal.pone.0258842](https://doi.org/10.1371/journal.pone.0258842).
- [34] Y.-J. Guan, Y. Ge, H.-X. Sun, S.-Q. Yuan, and X.-J. Liu, "Low-frequency, open, sound-insulation barrier by two oppositely oriented Helmholtz resonators," *Micromachines*, vol. 12, no. 12, p. 1544, Dec. 2021, doi: [10.3390/mi12121544](https://doi.org/10.3390/mi12121544).
- [35] F. Mizukoshi and H. Takahashi, "Tunable planar acoustic notch filter utilizing pneumatic deforming Helmholtz resonator array," in *Proc. IEEE 35th Int. Conf. Micro Electro Mech. Syst. Conf. (MEMS)*, Jan. 2022, pp. 849–851.
- [36] J. W. S. B. Rayleigh, *The Theory of Sound*. London, U.K.: Macmillan, 1896.
- [37] U. Ingard, "On the theory and design of acoustic resonators," *J. Acoust. Soc. Amer.*, vol. 25, no. 6, pp. 1037–1061, Nov. 1953, doi: [10.1121/1.1907235](https://doi.org/10.1121/1.1907235).
- [38] M. Alster, "Improved calculation of resonant frequencies of Helmholtz resonators," *J. Sound Vib.*, vol. 24, no. 1, pp. 63–85, 1972, doi: [10.1016/0022-460X\(72\)90123-X](https://doi.org/10.1016/0022-460X(72)90123-X).
- [39] A. Selamet and Z. L. Ji, "Circular asymmetric Helmholtz resonators," *J. Acoust. Soc. Amer.*, vol. 107, no. 5, pp. 2360–2369, May 2000, doi: [10.1121/1.428622](https://doi.org/10.1121/1.428622).
- [40] A. Peiffer, M. Grunewald, and P. Lempereur, "Comment on 'A lightweight yet sound-proof honeycomb acoustic metamaterial' [appl. phys. lett. 106, 171905 (2015)]," *Appl. Phys. Lett.*, vol. 107, no. 21, Nov. 2015, Art. no. 216101, doi: [10.1063/1.4936237](https://doi.org/10.1063/1.4936237).



FUMIYA MIZUKOSHI was born in December 1998. He received the bachelor's degree from Keio University, in 2021. He is currently pursuing the master's degree with the Takahashi Laboratory, Graduate School of Integrated Design Engineering, Keio University. His research interests include acoustic filters and their application.



HIDETOSHI TAKAHASHI (Member, IEEE) received the bachelor's, master's, and Ph.D. degrees from The University of Tokyo, in 2006, 2008, and 2011, respectively.

He was a JSPS Research Fellow at The University of Tokyo, from 2008 to 2011. From 2015 to 2019, he was an Assistant Professor at the Department of Mechano-Informatics, Graduate School of Information Science and Technology, The University of Tokyo. Since 2022, he has been an Associate Professor with the Department of Mechanical Engineering, Faculty of Science and Technology, Keio University. His research interest includes microelectromechanical systems related to force sensors.

• • •